Distribution Agreement

In presenting this thesis as a partial fulfillment of the requirements for a degree from Emory University, I hereby grant to Emory University and its agents the non-exclusive license to archive, make accessible, and display my thesis in whole or in part in all forms of media, now or hereafter now, including display on the World Wide Web. I understand that I may select some access restrictions as part of the online submission of this thesis. I retain all ownership rights to the copyright of the thesis. I also retain the right to use in future works (such as articles or books) all or part of this thesis.

Michelle Kwon Lee December 6, 2023

Morphology Engineering: Uncovering the Supramolecular Codes for Chirality

by

Michelle Kwon Lee

Dr. David Lynn
Adviser

Chemistry

Dr. David Lynn

Adviser

Professor Brenda Harmon

Committee Member

Dr. John Bacsa

Committee Member

2023

Morphology Engineering: Uncovering the Codes for Supramolecular Chirality

By

Michelle Kwon Lee

Dr. David Lynn

Adviser

An abstract of
a thesis submitted to the Faculty of Emory College of Arts and Sciences
of Emory University in partial fulfillment
of the requirements of the degree of
Bachelor of Science with Honors

Chemistry

2023

Abstract

Morphology Engineering: Uncovering the Codes for Supramolecular Chirality
By Michelle Kwon Lee

Supramolecular assemblies are found in various areas of nature, serving highly functional roles in both essential biological pathways as well as in various disease states. One notable peptide with self-assembly capabilities is $A\beta_{42}$, a major isoform of amyloid β that is associated with the formation of amyloid plaques in Alzheimer's disease. Here, characterization of various derivatives of the nucleating core of $A\beta_{42}$ ($A\beta_{16\text{-}22}$), including E22 (KLVFFAE), E22L (KLVFFAL), and E22V (KLVFFAV), has revealed supramolecular chiral structures with differing left- and right-handed twists. In addition to any external factors that may direct assembly chirality, we seek to uncover the design rules that dictate such inversions in peptide assemblies and establish a foundation for engineering tunable biomaterials that may be used for therapeutic purposes, including drug delivery. To achieve this, we designed a simpler peptide system where we expanded the phenylalanine sequence of the nucleating core, $A\beta_{16\text{-}22}$, to a 4F system which was found to have temperature dependent supramolecular chiral inversion. The 4F system peptide was then co-assembled with Doxorubicin and subsequently heated, resulting in precise and effective drug release. The ability to engineer the morphology of these supramolecular chiral structures underscores the importance of understanding design principles as self-assembling peptides take on a greater role in the design of therapeutics and various other applications.

Morphology Engineering: Uncovering the Codes for Supramolecular Chirality

By

Michelle Kwon Lee

Dr. David Lynn

Adviser

A thesis submitted to the Faculty of Emory College of Arts and Sciences
of Emory University in partial fulfillment
of the requirements of the degree of
Bachelor of Science with Honors

Chemistry

2023

Acknowledgements

First, I'd like to thank my advisor Dr. David Lynn. Thank you for your faith in my abilities as a scientist. Despite the ups and downs in my project, you stood steadfast in your confidence in me. You provided great advice and encouraged me to take my own path of exploration.

Second, I'd like to give specific thanks to Professor Brenda Harmon, Dr. Reza Saadein, and Dr. Deepika Das from Oxford for fostering my love of chemistry in my first two years of college. They went above and beyond to ensure that even the most basic concepts in chemistry were enjoyable to learn. I'd also like to thank them for giving me the opportunity to explore my love of teaching and mentoring and trusting me with guiding their students. Additionally, I give thanks to all my professors, who have helped me become the scientist I am today; to encourage my curious nature and celebrate the joys of learning with me.

Third, I'd like to thank Dr. John Hartwig and Eric Kalkman from Berkeley for giving me my first chance at working in a lab. Despite the COVID restrictions and the fact that I had just finished my freshman year, they took me under their wing and helped build my confidence in designing and executing new projects. I recognize that my contributions to the research there were likely minimal, but they continued to unconditionally encourage me in my attempts to provide good data.

Fourth, I'd like to thank Dr. John Bacsa for giving me the chance to work at the X-ray crystallography center. It was a completely different landscape from the type of chemistry and equipment that I am used to working with and helped broaden the scope of my chemistry knowledge. He has helped me discover that physical chemistry can be very interesting and has many more applications than I could ever have thought of.

Fifth, I'd like to thank all the graduate and undergraduate students of the Lynn Lab, as well as my friends for their support. My lab mates never hesitated to teach me new techniques or help me with my various struggles in the lab. Their critique and feedback were critical to my success, and they were always available to help me work through my mistakes.

Sixth, I'd like to thank my family. They have stood by my side for all the ups and downs of college with unwavering support. They encourage me to explore and have continuously listened to my ramblings about my research, despite the fact that it is a wholly unfamiliar field to them.

Finally, I'd like to thank the Freeman Lab at the University of North Carolina at Chapel Hill. Without them, this thesis and our collaborative paper would not have been possible. This thesis was adopted from the Lynn Lab-Freeman Lab collaborative paper: Uncovering Supramolecular Chirality Codes for the Design of Tunable Biomaterials, in review at Nature Communication.

Table of Contents

Table of Figures

Introduction

Supramolecular structures and assemblies are found to have high degrees of functionality in natural systems, playing critical roles in many cellular activities as well as being implicated in various disease states.[1,2] β-sheet rich protein amyloid aggregates, for example, are associated with numerous neurodegenerative diseases including Alzheimer's Disease (AD).[3,4] Interestingly, there is substantial evidence to indicate that many polypeptides are able to form amyloids under the appropriate conditions,[5-7] and much of amyloid morphology is directed by both sequence and assembly conditions.[8,9,W] Even single amino acid modifications are capable of influencing peptide registry, and various assembly conditions are capable of yielding an array of different assembly morphologies.[8,10-12,W]

In the case of yeast, such single amino acid modifications can define species barriers between closely related yeast species.[13,14] β-sheet rich aggregates, in the form of prions in yeast cells, control a wide array of functions, including acting as heritable elements.[15-19] Like DNA, these heritable elements can encode and transmit stable phenotypic information; however, they do so via distinct amyloid conformations.[19] These morphologically different amyloids therefore act as different "strains" that distinguish one yeast species from another.[15,17,18] This phenomenon thus emphasizes the importance of understanding how peptide modifications, even as small as a single amino acid substitution, establish different accessible amyloid conformations.

Further, the etiologies behind many diseases have been found to be from various prions (abnormally folded proteins) and amyloids.[4,20,21] Specifically, amyloids have been implicated in the disease pathologies of Alzheimer's disease, Parkinson's disease, and Huntington's disease,

among many others.[4] Such amyloids are often found to have secondary β-sheet structures and are particularly resistant to degradation via standard metabolic pathways in the body,[4,22] both properties contributing to the formation of aggregate deposits.[23]

Prions, likewise, have been implicated in diseases pathologies, often within animals, including Scrapie, chronic wasting disease, and bovine spongiform encephalopathy (more commonly known as Mad Cow's Disease).[4,20,21] Some prion diseases found in humans include fatal familial insomnia, Creutzfeldt-Jakob disease (CJD), variant CJD, and Kuru.[20,21,24] As per its namesake, Prion Protein (PrP) is one of the most infectious sources of misfolded proteins that can cause some of these diseases, although it is not the only protein to be able to do so.[21,25] In particular, prions are notable for their ability to act as infectious agents by causing other proteins to misfold, propagating the formation of more prions, within an organism or as a vector to another organism.[21,25,26] This vector can be from animal to animal, such as in mad cow's disease; animal to human, such as in the case of bovine spongiform encephalopathy potentially causing variant CJD; or human to human, such as in Kuru, where the disease is spread via ritual cannibalism.[20,21,27] Most often, the vector of transmission tends to be via consumption of contaminated tissue, but can also be inherited, such as in the case of fatal familial insomnia.[20,28] In both amyloid and prion associated diseases, devastating and often fatal neurodegenerative deterioration is observed in almost all cases.[4,20]

Various factors, including temperature and sequence, are capable of affecting the assembly process of many supramolecular assemblies.[8,W] One model that is used to represent how some peptides assemble is known as the two-step nucleation process: 1) peptides are dissolved in

solution; 2) peptides nucleate to form a particle (first nucleation), phase separation occurs; 3) nucleation of the peptide occurs (second nucleation) and assembly formation begins inside the particle; 4) assemblies propagate until all peptides in the particle are consumed.[8] Differences in pH, solvent systems, ions, and external templates are all capable of affecting the assembly rates, stability, and final morphologies of the assembled system, in part by causing different nuclei to form.[8]

Within the realm of supramolecular structures, supramolecular chirality (also referred to as suprahelicity) has been found to be a prevalent and, often, highly functional feature that is found in many biological systems and assemblies.[1] Such chiral or helical structures are often stabilized via weak, and thus temporary, intermolecular interactions such as hydrogen bonding, electrostatics, π stacking, and van der Waals forces.[29] This results in helical structures that are capable of supramolecular chiral interconversion between left- and right-handed forms, giving rise to high levels of biofunctionality.[29] For example, in the case of DNA isoforms, Z-form DNA has been found to have higher binding affinity than B-form DNA to certain proteins such as RNA adenosine deaminase, a nuclear-RNA-editing enzyme, as well as E3L, a protein associated with poxvirus pathogenicity; both are relevant in gene expression pathways.[30] Supramolecular chirality dependent biofunctionality is also observed in motile bacteria, where a left- to right-handed inversion of the helical flagella controls its standard-swimming and chaotic-tumbling motions.[31]

In particular, supramolecular chirality is commonly observed in a variety of protein and peptide systems, including linear proteins, tubular proteins, and protein cages: actin fibers, the tobacco

mosaic virus capsid, and rat vault shells being several well-known examples.[1] Such protein structures can often achieve high levels of biofunctionality as a result of suprahelical conversion between left- and right-handed structures.[29] For example, in the case of $A\beta_{40}$ (amyloid β, residue 1-40), amyloid fibers isolated from Alzheimer's disease (AD) brain tissue showed opposing supramolecular chirality to $A\beta_{40}$ amyloid fibers assembled *in vitro*.[23] Characterization via cryo-EM reveals that when $A\beta_{40}$ amyloid fibers are assembled *in vitro*, a left-handed twist is observed, whereas in fibers isolated from brain tissue, a right-handed twist is observed.[23] When exposed to proteinase K, these right-handed fibers showed higher resistance to degradation, which may be associated with amyloid accumulation in AD plaques resulting in disease progression,[23] thus indicating that disease pathology may be influenced by the fiber's supramolecular chirality.

This type of biofunctionality arising from supramolecular chiral structures becomes a source of high potential in the design and application of controllable biomaterials. To do so, however, requires a well-established understanding of the factors that dictate the formation of supramolecular chiral structures as well as the cause of chiral inversion. Numerous studies have explored the effects of peptide sequence, pH, solvent systems, ions, external templates, and other factors on assembly morphology, and more specifically, supramolecular chirality.[8,32-35,W] For example, a mutation of the second phenylalanine (F) to a tryptophan (W) in the peptide Fmoc-FFX (X=amino acid H, R, S, E, or D) has been found to result in the conversion of left-handed helical assemblies into right-handed helical assemblies.[32] The assembly of the amyloid protein α-synuclein (AS), specifically AS_{71-82}, into left- or right-handed morphologies is dependent on the overall peptide concentration and the peptide:lipid molar ratio when assembled in the presence of anionic lipid vesicles.[33] Multiple studies have found the polarity of the solvent directs either a

left- or right-handed twist in supramolecular chiral structures assembled from non-peptide organic molecules.[34] In another study, researchers were able to invert the supramolecular chirality of an organic molecule-based assembly of cholesteric liquid crystals via laser irradiation of 808 nm or 980 nm wavelength light, forming left- and right handed assemblies, respectively.[35]

Additionally, temperature dependent experiments and computational studies help reveal the kinetic-thermodynamic properties of left- and right-handed supramolecular chiral assemblies.[36-38] Temperature-induced inversion of supramolecular chiral assemblies is regulated by an energy barrier separating the left- and right-handed morphologies, with each morphology corresponding to either a kinetically trapped or thermodynamically favored state.[36-38] Additional computational analysis reveals the right-handed twists to be the thermodynamically favored morphology, with inversions from the left- to right-handed state being directed by the assembly's ability to overcome this respective energy barrier.[36-38] It should be noted that an assembly may melt before overcoming this barrier and undergoing suprahelical inversion.

Supramolecular assemblies are investigated using various techniques that probe the assembly's structure, electrostatics, packing, chirality, and other features of the structure. Some of the most common techniques include TEM, SEM, FRAP, IR, NMR, electron and X-ray diffraction (ED and XRD), cryo-EM, and CD. Transition electron microscopy (TEM) and scanning electron microscopy (SEM) uses a beam of electrons to show the cross-sectional structure or surface of the structure, respectively. In fluorescence recovery after photobleaching (FRAP), fluorescent emissions and variations in emission values are measured before and after exposure to high intensity light. The recovery time of fluorescence emissions can be used to distinguish assemblies in either liquid-

like or particle states, versus a more solid assembly, where a lack of recovery is associated with more solid, rigid structures.[39] Infrared spectroscopy (IR), nuclear magnetic resonance (NMR), and electron or X-ray diffraction (ED or XRD) are all used to obtain properties such as interstrand distances, secondary structures, bond types, registry, helical twists, and other structural information. However, these techniques individually are not capable of yielding absolute structure and are often used in conjunction with other methods of structure determination such as Cryo-electron microscopy (Cryo-EM). In conjunction with structural information obtained by the previously mentioned methods, Cryo-EM can create high resolution models of assemblies or proteins of interest. In addition to all of these, one of the most important techniques in the study of supramolecular chirality is circular dichroism (CD). CD uses polarized light and the corresponding optical activity of a compound to determine the coupling angles between the amide bonds, the ϕ and ψ angles specifically.[40,41] This technique can further be used to determine both β-sheet chirality and ultimately supramolecular chirality.[41]

Here we explored a peptide sequence which constitutes the core β-sheet assembly domain of $A\beta_{42}$, the major isoform of amyloid β associated with the formation of amyloid plaques in Alzheimer's disease.[3] The peptide, known as E22, is the 16-22 residues of $A\beta_{42}$, with the sequence KLVFFAE. Morphology changes associated with variations of the C-terminus as well as solvents and assembly conditions are observed; electron microscopy, ED, CD, and NMR reveal supramolecular chiral inversion following certain C-termini modifications and morphology changes with varying solvents and assembly conditions.

Additionally, we sought to further explore the nucleating core of E22: the FF sequence. Diphenylalanine (FF) is a short peptide sequence that is found to promote self-assembly in many peptide systems.[42] FF-based peptides assemble into a variety of structures from nanotubes to nanofibrils to vesicles, as well as form inorganic hybrids with other molecules.[42] To probe the change in supramolecular chirality observed in the E22 system, a peptide representing an extended nucleating core, 4F, was synthesized. The 4F peptide consists of an Fmoc protected N-terminus, 4 phenylalanines, and a PEG_2 C-terminus. Interestingly, this peptide was found to have temperature dependent inversion of supramolecular chirality.

This type of tunable supramolecular chirality and temperature dependence is noteworthy in engineering and the development of novel drug delivery systems. We found the properties of the 4F peptide assembly to be ideal for both potential drug transport and subsequent removal from the body. The aromatic rings found in the sequence are useful in the incorporation of drugs with conjugated multi-ring systems, such as doxorubicin (DOX). As such, we investigated the ability of the 4F peptide to incorporate DOX into assembly as well as its ability to thermally control the release of DOX.

Uncovering the codes for supramolecular chirality can help define the mechanism behind the assembly of chiral structures, allowing us to better design treatments for certain disease pathologies or discover ways to use supramolecular chirality as a marker or target for treatment. Additionally, further probing will lead to the understanding of the significance of certain chiral structures in diseases, from its stability to its contribution to the pathology's mechanisms. Uncovering the code for supramolecular chirality also unlocks the potential for synthesizing new

biomaterials, helps establish our understanding of the complexity of the beginnings of life, and helps engineer novel, biofunctional materials.

Results and Discussion

Sequence Dependent β-Sheet Nucleation Directs Supramolcular Chiral Assembly: The E22 System

The two-step nucleation model provides a remarkable degree of access to various supramolecular structures via its meta-stable particle phase and dynamic activity with the environment. The peptide sequence comprising the core β-sheet domain of $A\beta_{42}$ (herein referred to as E22 or KLVFFAE) employs three different mechanisms for assembly growth and propagation: H-bonding along the backbone which generates β-sheet secondary structures, β-sheet stacking which generates a cross-β architecture, and leaflet association which generates higher order peptide assemblies.[43-47] Each mechanism can be modulated by variations in the two-step nucleation model, ultimately resulting in morphological changes.

The E22 peptide, with the sequence KLVFFAE, assembles to form homogeneous bilayer nanotubes under acidic condition, which results in the protonation of the terminal E residue. This is in contrast to E22 assembled at neutral pH, which produces fibers.[43,48] The formation of different morphologies may be caused by cross-strand pairing interactions of lysine16-glutamate22, where the presence or absence of the salt bridge between the lysine and glutamate directs its assembly. Removal of the salt bridge via substitution or acidic conditions results in nanotube assemblies.[45] To further probe this pH dependent interaction, the terminal glutamate was substituted with a leucine (herein referred to as E22L or KLVFFAL) and assembled in 40% acetonitrile solution with 0.1% trifluoroacetic acid (TFA) for acidic conditions. Leucine was chosen for its hydrophobic residue that closely matched the structure and steric profile of glutamate. The resulting peptide was likewise found to assemble into homogeneous bilayer nanotubes.[W]

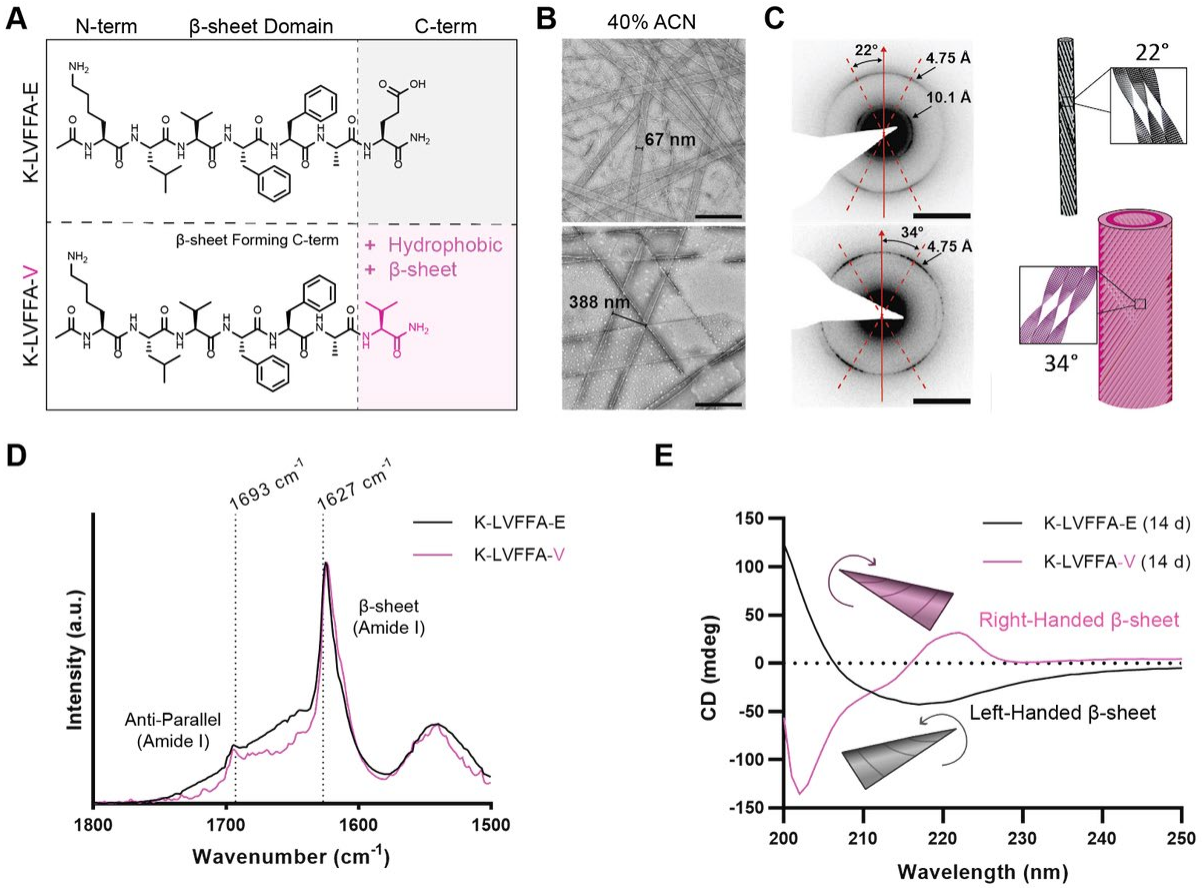

Figure 1. (A) the structures of KLVFFAE (E22) and KLVFFAV (E22V); (B) TEM images of peptides assembled in 40% ACN, 0.1% TFA for 2 weeks, scale bars = 500 nm; (C) Electron diffraction of the peptides, scale bars = 2 nm^{-1} and schematic of the helical twist of the tube; (D) IR of E22 and E22V; (E) CD spectra of mature E22 and E22V[W]

The terminal E/L residue was also substituted with valine (herein referred to as E22V or KLVFFAV) due to the amino acid's prevalence in β-sheet formation (Figure 1A).[49] This peptide sequence also assembled into bilayer nanotubes. However, the corresponding one methylene reduction on the C-terminus residue resulted in a radically different cross-sectional area. The E22V peptide yielded a nanotube with a diameter of 397 ± 52 nm, which is over 5 times larger than the E22 peptide nanotube with a diameter of 72 ± 5 nm (Figure 1B). Additionally, while electron diffraction also

confirmed the cross-β architecture of both nanotubes, the E22V nanotubes were revealed to have a greater helical twist at 34° compared to the E22 nanotube that has a helical twist of just 22° (Figure 1C). Characterization of the cross-β architecture reveals 4.7 Å d-spacing from H-bonded β-sheet strands in all nanotube assemblies. However, 10.1 Å d-spacing from extended β-sheet stacking is observed only in E22 and E22L assemblies, not in E22V assemblies. This absence may be due to distortion and flattening of the wide E22V nanotube. Sharp reflections at 4.7 Å d-spacing and a sharp but broader peak at around 10-11 Å d-spacing are also observed in E22 and E22L powder X-ray diffraction data, corresponding to the data from the electron diffraction (Figure 2). Additionally, a very broad, low-resolution peak between 9-13 Å d-spacing is observed in the E22V spectrum (Figure 2). Like the electron diffraction, this broad peak may be reflective of nanotube distortion or a smaller number of laminated β-sheet lattice repeats.

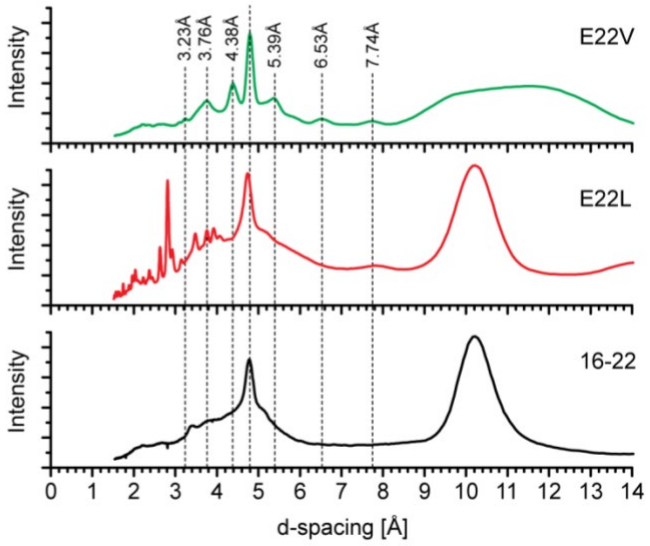

Figure 2. Powder XRD of E22 system assembled peptides[X]

FT-IR analysis showed similar amide-I bands at 1627 cm^{-1} and 1693 cm^{-1}, indicating that both the E22 and E22V peptides assemble into anti-parallel β-sheets (Figure 1D). To investigate peptide registry, assemblies of [1-^{13}C]V18 [^{15}N]A21 isotopically enriched E22, E22L, and E22V were characterized via solid-state NMR. Solid-state NMR ^{13}C-^{15}N distance measurements for all three

peptide nanotubes assembled under acidic conditions correspond to distances that are characteristic of out-of-register antiparallel β-sheets.[W]

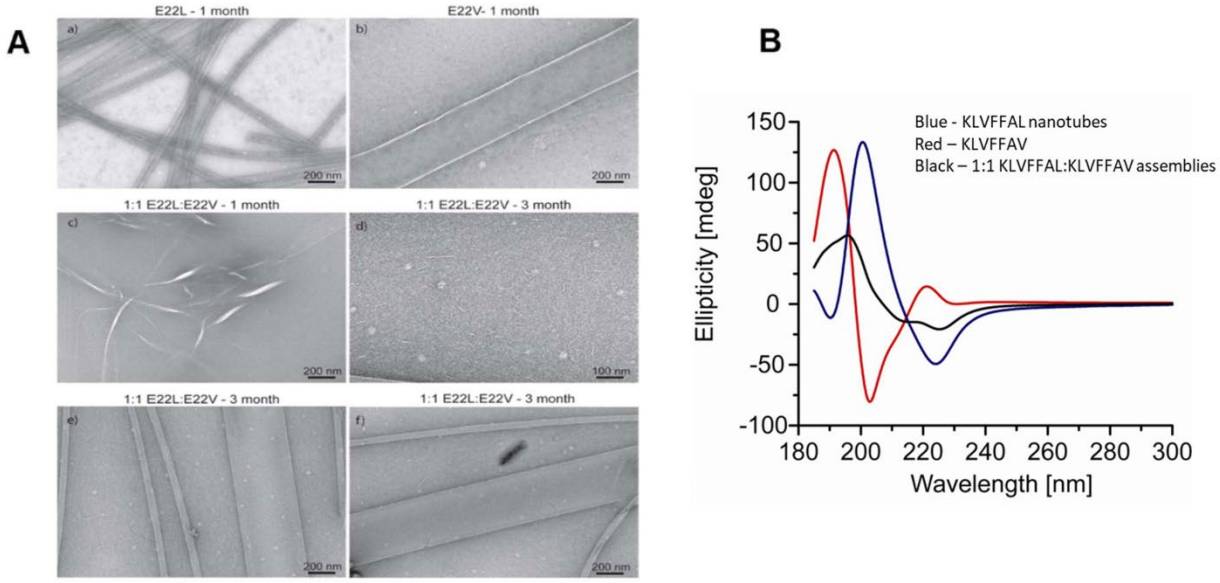

Figure 3. (A) TEM of individual E22L assemblies, E22V assemblies, and E22L/V co-assemblies at 1 month and 3 months; (B) CD of individual E22L and E22V assemblies as well as the E22L and E22V co-assembly[W]

The most notable difference in the E22 and E22L nanotubes versus the E22V nanotubes was observed via circular dichroism (CD). While the CD spectra indicated that both E22/E22L and E22V nanotubes formed β-sheets, the red-shifted β-sheet transition at around 220 nm shows opposite signs. E22 and E22L nanotubes both show a local minimum at around 220 nm whereas E22V nanotubes show a local maximum at around 220 nm, corresponding to left- and right-handed helicity, respectively (Figure 1E, 3B). To help determine whether this change in handedness is caused by differential nucleation of left- versus right-handed nanotubes during two-step nucleation, co-assemblies of E22L and E22V were assessed. The two peptides were mixed

together at a 1:1 ratio and allowed to incubate for one month. After one month, the co-assembly formed a heterogeneous mixture of filaments and sheets, observed by TEM (Figure 3A, c). After further incubation, a heterogeneous mixture of small tubes, large tubes, and short filaments was observed (Figure 3A, d-f). CD measurement of this 1:1 mixture appears to be a simple summation of individual E22L and E22V nanotube spectra (Figure 3B). These results indicate distinct nucleation events for each of the products: the large nanotubes, the small nanotubes, and the fibrils. The nanotubes are likely standard E22L and E22V nanotubes whereas the fibrils likely account for E22L and E22V co-assembly.

The role of electrostatics, solvent, and temperature effects on distinct nucleation events were also investigated. In addition to E22 and E22V, the peptide KLVFFA-PEG_2 was synthesized, where the PEG_2 moiety is used to remove any electrostatic effects and β-sheet interactions while retaining E22's hydrophilic properties (Figure 4A). When assembled in HFIP, both E22 and E22V assemble into ribbons after 2 hours whereas in KLVFFA-PEG_2, assembly is not observed beyond small amounts of aggregates (Figure 4B). These peptides were then annealed (heated to 95°C and cooled at 1°C/min), after which bundles and nanotubes were observed for E22 and E22V, respectively (Figure 4C). However, only larger aggregates are observed in KLVFFA-PEG_2. Unlike the C-terminus modifications to E22L and E22V, no distinct assembly or change is reflected in the KLVFFA-PEG_2 peptide. Thus, this peptide was not explored further.

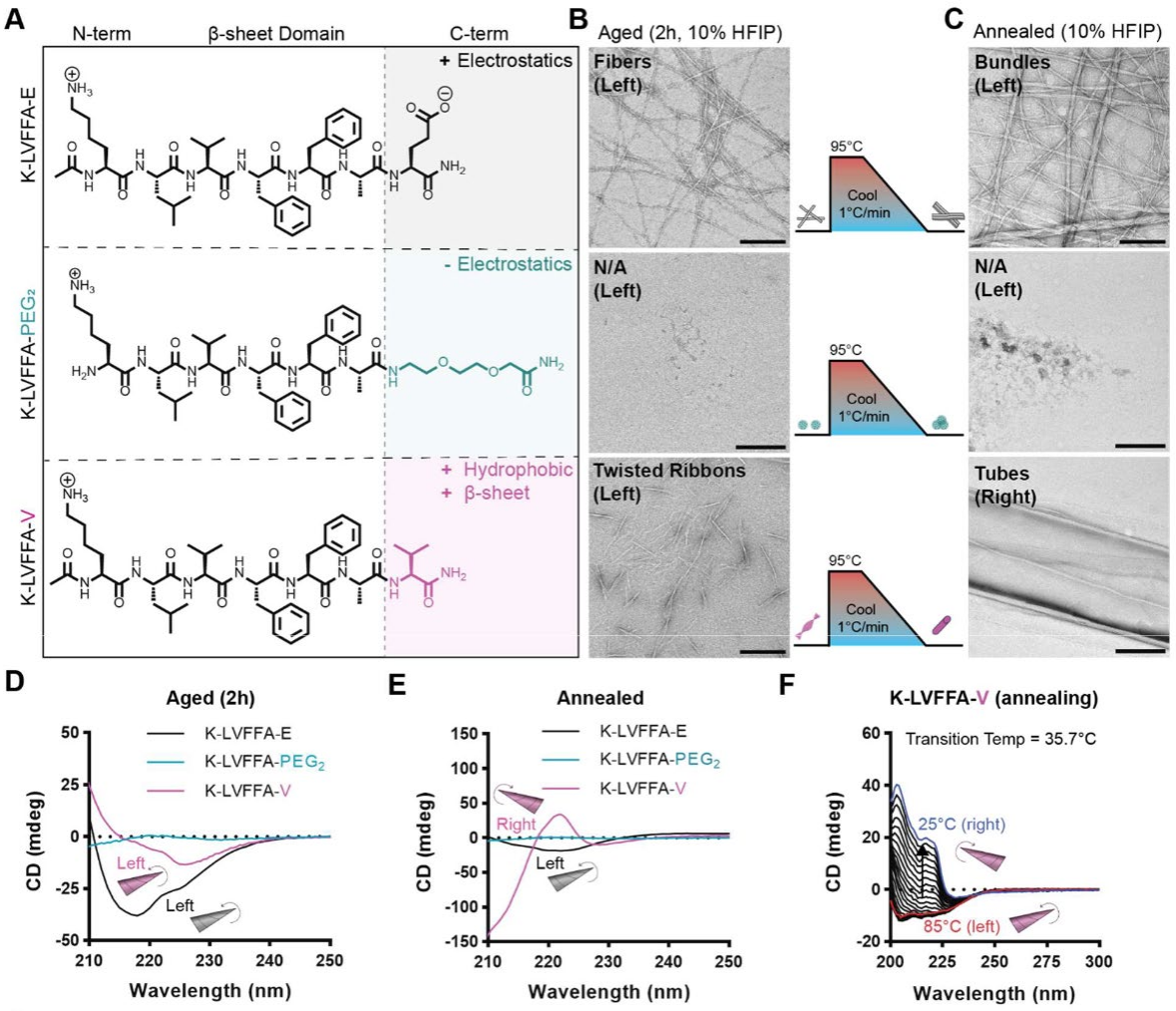

Figure 4. (A) the structures of E22, KLVFFA-PEG_2, and E22V; (B) TEM images of aged peptides in 10% HFIP; (C) TEM images of annealed peptides in 10% HFIP; (D) CD spectra of aged assembly; (E) CD spectra of annealed assembly; (F) CD spectra of E22V during slow cooling[W]

CD spectra of the assemblies reveal that both the E22 and E22V assemblies in HFIP consisted of left-handed β-sheets when aged (Figure 4D). However, when annealed, the HFIP assembly of E22V shows inversion of chirality into a right-handed assembly (Figure 4E). The helical inversion, monitored by CD, revealed that the right-handed transition occurred not during the heating, but during the slow cooling process (Figure 4F). Nanotube assemblies of E22 and E22V assembled in ACN were also heated to 95°C and allowed to cool to room temperature. The resulting TEM

images at 95°C and after cooling show reformation of nanotube-like structures for E22V and the presence of fiber-like structures, but no reformation of any nanotube-like structure for E22 (Figure 5A).

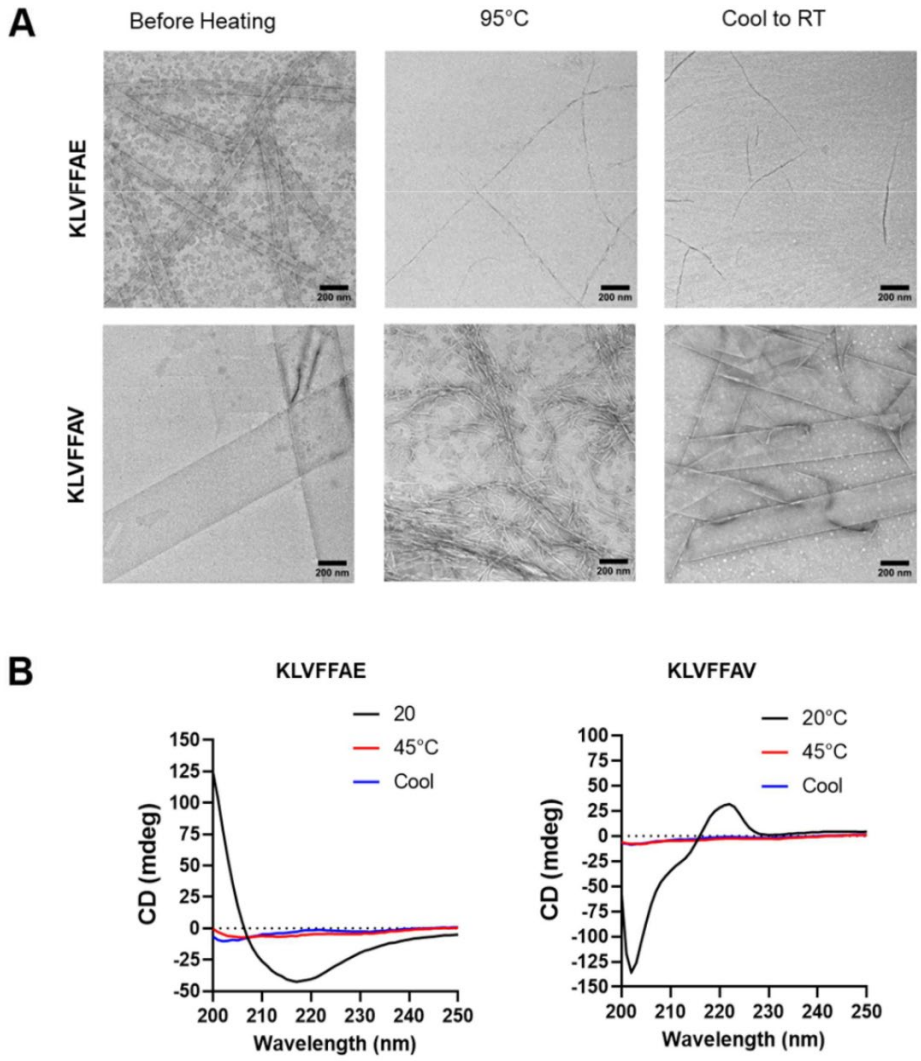

Figure 5. (A) TEM images of E22 and E22V assemblies in ACN before, during, and after heating; (B) CD spectra of E22 and E22V assemblies before, during, and after heating. Peptides were heated until CD signal stopped changing[W]

Interestingly, despite the apparent presence of sheets and nanotube-like structures for E22V under TEM, CD does not show recovery during any heating and subsequent cooling (Figure 5B).

From these results, we posit that distinct and different nucleation events occur based on differing environmental conditions. Firstly, we observe a change in the assembly rates of E22 and E22V in different solvent systems, where HFIP promotes faster assembly rates than ACN.[W] Additionally, heating is required to overcome the energy barrier leading to a distinct right-handed nucleation event, and slow cooling is required to allow a stable right-handed nucleation point to occur. In the case of the ACN assembly, the higher organic solvent content may provide both reduced hydrophobic interactions and stronger β-sheet interactions, allowing nanotube formation at room temperature.[50] Further, if β-sheets are already nucleated in the right-handed state, unregulated rapid cooling can occur and still allow the nanotubes to reform after melting. However, in the case of the left-handed structures, reformation will not occur. Thus, we find that solvent, temperature effects, and C-terminus amino acid interactions can be used to modulate the nucleation and growth of helical β-sheet assemblies.

Expansion of Nucleating Core: The 4F System

In order to further probe the temperature dependent effects on regulating supramolecular chirality, the nucleating core of E22, diphenylalanine (FF), was isolated and expanded to create the 4F peptide system. Initial experimentation of the 4F system consisted of exploring N-terminus modifications on morphology. The peptides K-FFFF-PEG_2, H_2N-FFFF-PEG_2, and Fmoc-FFFF-PEG_2 were synthesized, each to account for either a charged N-terminus, a truncated N-terminus, or, following the motif of aromatic phenylalanines, an aromatic N-terminus (Figure 6A).

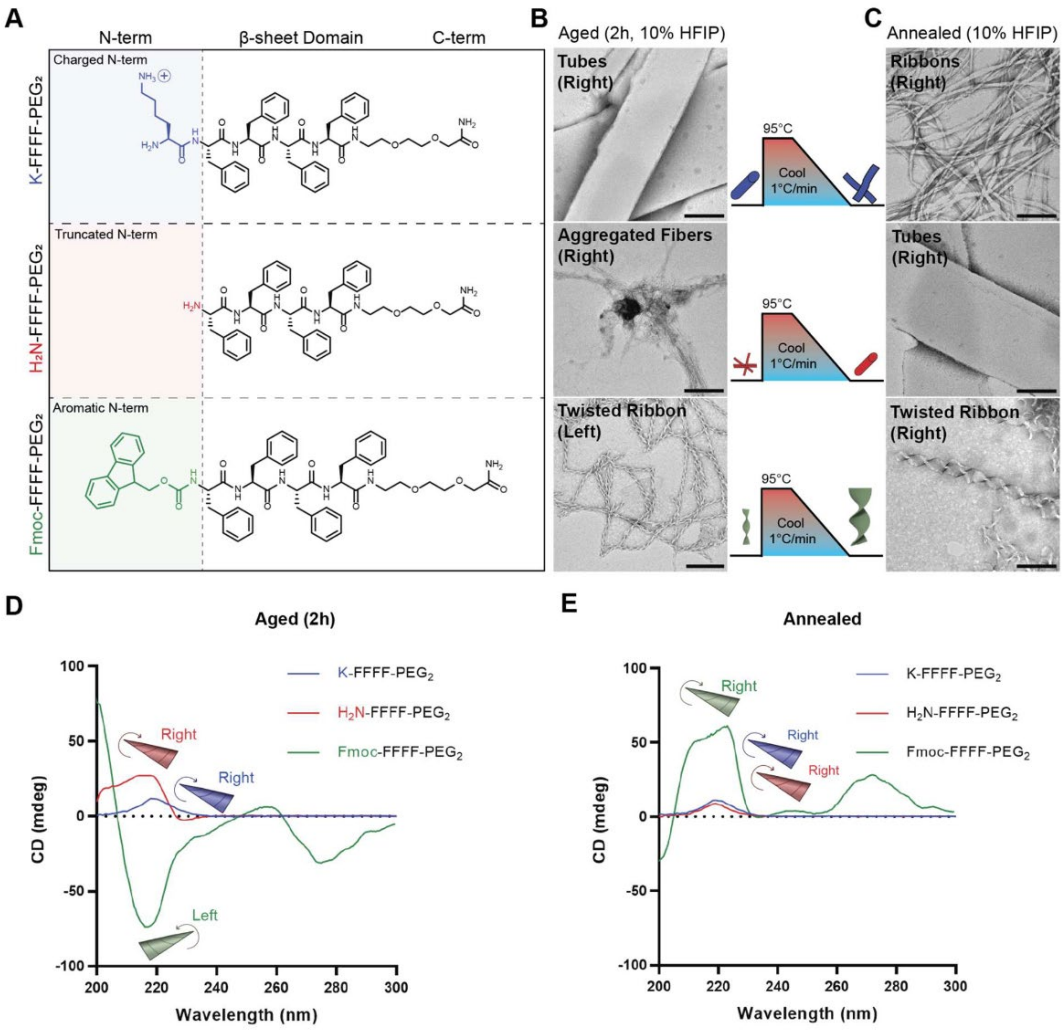

Figure 6. (A) the structures of K-FFFF-PEG_2, H_2N-FFFF-PEG_2, and Fmoc-FFFF-PEG_2; (B) TEM images of aged peptides in 10% HFIP; (C) TEM images of annealed peptides in 10% HFIP; (D) CD spectra of aged assembly; (E) CD spectra of annealed assembly[W]

The peptides were assembled in HFIP for 2 hours, then subsequently annealed. CD spectra after aging revealed that both K-FFFF-PEG_2 and H_2N-FFFF-PEG_2 assemblies consist of right-handed β-sheets and Fmoc-FFFF-PEG_2 assemblies consist of left-handed β-sheets (Figure 6D). After annealing, CD revealed that all three peptides consist of right-handed β-sheets, indicating a temperature dependent suprahelical inversion of the Fmoc-FFFF-PEG_2 assembly (Figure 6E). Additionally, morphology changes are observed from each of the peptide assemblies following

the annealing process: K-FFFF-PEG_2 transforms from tube like structures to ribbons, H_2N-FFFF-PEG_2 transforms from aggregated fibers to tube like structures, and Fmoc-FFFF-PEG_2 transforms from a left-twisted thin ribbon to a right-twisted thick ribbon (Figure 6B, 6C). These experiments provide insight into the morphological control of assembly that can be achieved via N-terminus modification.

Following the observation that Fmoc-FFFF-PEG_2 assemblies have temperature dependent suprahelical inversion, C-terminus modifications of this 4F variant were explored. The additional peptides Fmoc-FFFF-PEG_2-Kaz and Fmoc-FFFF-PEG_2-Cys were synthesized, one containing an azide functional group and the other containing a thiol functional group, respectively (Figure 7A). The peptides were assembled in HFIP for 2 hours then subsequently annealed. CD data and TEM both reveal that all aged assemblies exhibit a left-handed twist which inverts after heating (Figure 7C). Interestingly, the right-handed ribbon that resulted from annealing was thicker than the original left-handed ribbon for all three peptides (Figure 7B). It is also interesting to note that while the general morphologies of the aged and annealed ribbons are nearly identical across all three peptides, the transition temperature for suprahelical inversion differs (Figure 7B, 7D). Fmoc-FFFF-PEG_2-Kaz has a transition temperature around 22.8°C, Fmoc-FFFF-PEG_2 has a transition temperature around 35°C, and Fmoc-FFFF-PEG_2-Cys has a transition temperature around 45.1°C (Figure 7D). Unlike modifications on the N-terminus, modifications on the C-terminus appear to modulate the thermodynamic barrier between left- and right-handed states.

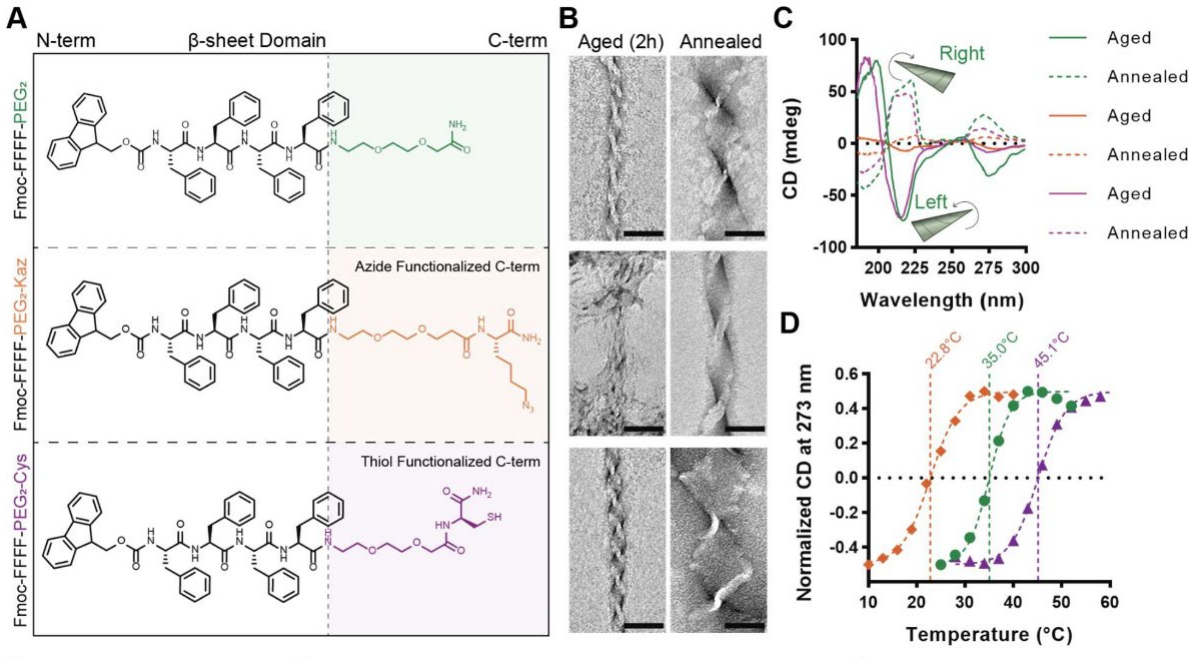

Figure 7. (A) the structures of K-FFFF-PEG$_2$, Fmoc-FFFF-PEG$_2$-Kaz and Fmoc-FFFF-PEG$_2$-Cys; (B) TEM images of aged and annealed peptides in 10% HFIP; (C) CD spectra of aged and annealed assembly; (E) CD spectra of transition temperatures[W]

While the initial and final products have been characterized and shown to have gone through supramolecular chiral inversion, uncovering the mechanism for how such chiral inversions occur is also critical in developing methods to engineer tunable peptides. One model that may be used to represent the mechanism through which supramolecular chiral inversion occurs is the previously discussed two-step nucleation. Under this method, the application of heat results in the melting of the peptide and the reformation of a second nucleus or particle, where different supramolecular structures can be accessed and propagated. An alternative model proposes that the structures cooperatively untwist and retwist with inverted handedness.

The transition from the left- to right-handed ribbon of the Fmoc-FFFF-PEG$_2$ assembly was tracked via TEM imaging at different temperature points. The images suggest helical unwinding followed

by merging and retwisting occur, as the second model suggests (Figure 8). Supramolecular chiral inversion was also tracked in real time: confocal microscopy was used to observe assemblies that were stained with Thioflavin T (ThT), then heated.[W] The results indicate that the peptide network may be capable of contraction, but does not directly disassemble or reassemble. Additionally, we found that the wider ribbon structure of the annealed product is the result of structures laminating together to form the right-handed assembly.[W] Finally, fluorescence recovery after photobleaching (FRAP) was used to explore structural dynamics during chiral inversion, revealing that monomers become somewhat more mobile as the assembly approaches the transition temperature, and this mobility greatly increases at high temperatures.[W]

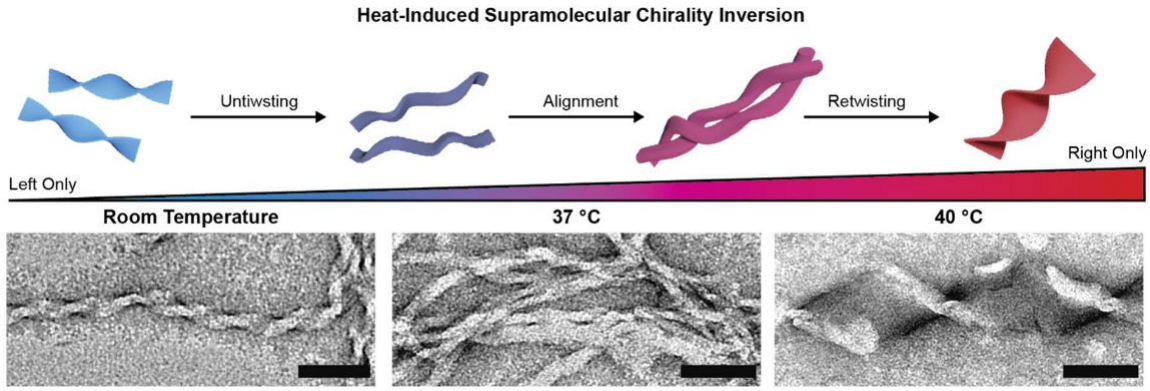

Figure 8. TEM progression of supramolecular chirality inversion of Fmoc-FFFF-PEG_2[W]

Drug Delivery Vehicle Morphology Engineering

The ability to thermodynamically control the suprahelical inversion of these peptides makes it of great interest in the development of new drug delivery systems. Fmoc-FFFF-PEG_2 is particularly notable for its physiologically relevant transition temperature of 35°C. As such, extensive characterization is performed to assess the peptide assembly's potential for drug delivery.

Chymotrypsin degradation assays were used to assess the suitability of Fmoc-FFFF-PEG_2 for biological applications. Both the aged and annealed (left- and right-handed) assemblies were exposed to chymotrypsin for 24 hours, and the resulting products were assessed via fluorescamine assay for degradation. Analysis of the assemblies by TEM after 24 hours shows significantly higher levels of degradation on the annealed (right-handed) assemblies than the aged (left-handed) assemblies (Figure 9). Degradation products were identified via HPLC and MS, revealing that the chymotrypsin primarily cleaved the Fmoc group from the peptide for the left-handed assemblies and the Fmoc-F group for the right-handed assemblies.[W] These results revealed that the left-handed assembly has higher resistance to degradation, possibly caused by differing peptide registries, which may affect the internal bond accessibility by chymotrypsin.

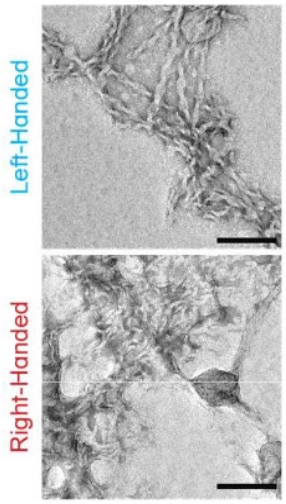

Figure 9. TEM of chymotrypsin degradation assay[W]

Next, we assessed the doxorubicin (DOX) loading capabilities of the Fmoc-FFFF-PEG_2 assembly. The aromatic rich structure of the peptide was suspected to be useful in the incorporation and retention of aromatic or ring-based drugs including DOX. The peptides were assembled in solutions of various DOX concentrations. We found the maximal DOX loading of the peptide to be 68.8 nmol DOX per µmol of peptide.[W] DOX release was measured using confocal microscopy where DOX fluorescence intensity could be observed.[W] Heating the assembly at 37°C for 1 hour resulted in a significant decrease in DOX intensity.[W]

Following this, we tested the ability of DOX release from assembly into cancer cells in culture. Fmoc-FFFF-PEG_2 was assembled in the presence of 5 μM DOX solution and any excess DOX was removed. The DOX-loaded assemblies were then added to cell cultures of HeLa and NDA-MB231-BR cells and left to incubate for 48 hours. Live-dead imaging showed a clear reduction in cell proliferation and greater cell death was observed, indicating efficient and high levels of DOX release (~60%).[W] Additionally, the Fmoc-FFFF-PEG_2 peptide is minimally toxic making it a good candidate for drug delivery.[W]

Conclusion

Uncovering the code for supramolecular chirality, unlocks the potential for synthesizing new biomaterials, provides further insight into the complex origins of life, and helps to better understand certain diseases. Here we specifically explore one avenue of potential tools, specifically therapeutics, that can be engineered with these principles. The incorporation of DOX into peptide assemblies or modulating the inversion of supramolecular chirality is hardly new. However, it demonstrates a vastly unexplored avenue of biofunctional tools with great potential, provided that there exist well established design rules for directing peptide assembly.

While we aim to provide a comprehensive review of modulating supramolecular chirality, this work is hardly exhaustive. In these studies, we sought to establish peptide codes that dictate assembly chirality, and to a lesser extent, morphology. As is, further characterization of the E22 and 4F peptide system must be achieved in order to understand the "why" and the "what" behind the differences in each of the left- or right-handed assemblies. Additionally, how is it that the removal or addition of just one methylene linker result in such a complete difference in both cross-sectional area and assembly chirality? Do all supramolecular chiral inversions follow the same model? And if not, what factors dictate which model the assembly transformation follows? It is distinctly possible that as more factors are assessed, libraries of dynamic peptide assemblies can be developed and provide a template for researchers to develop their own peptide system.

Further research into this area may also reveal more information on the "chaotic" nature of peptide behavior.[51] Peptide assembly plasticity, such as those explored in these experiments, allows a protein or peptide to adopt different forms based on different environments. Perhaps

this method of conformation adaptation based on environment was used to increase complexity at the beginnings of life. Despite this chaos, however, peptides do not have an infinite combination of folding possibilities and will fall into one energy trap or another. This “chaotic” side of peptides, especially in intrinsically disordered proteins (IDPs) can also be harnessed to make other biomaterials, especially those that require some type of dynamic responsiveness.[52,53]

For our work specifically, defining the mechanism behind the assembly of supramoleuclar chiral structures, allows us to better design treatments for certain disease pathologies or discover ways to use supramolecular chirality as a marker or target for treatment. Even further probing will lead to the understanding of the significance of certain chiral structures in diseases, from its stability to its’ contribution to the pathology’s mechanisms.

Methods

Foreword: The following methods and experiments were performed in conjunction with collaborators at the University of North Carolina Chapel Hill's Freeman Lab.

Materials

E22 Peptide System

Rink amide AM resin, TFA, Fmoc-Ala-OH and Fmoc-Glu-OH were purchased from Chem-Impex; Fmoc-Val-OH, Fmoc-Leu-OH, DIC, and Oxyma Pure were purchased from AnaSpec; Fmoc-Phe-OH was purchased from AAPPTec; Fmoc-Lys(Boc)-OH was purchased from MillporeSigma; N,N'-Diisopropylcarbodiimide (DIC) was purchased from AAPPTEC; thioanisole was puchased from TCI; piperidine, ethanedithiole, anisole, and acetic anhydride were purchased from Sigma Aldrich. L-amino acids were used to synthesize all peptides. All reagents were used as received.

4F Peptide System

Rink amide MBHA resin and Fmoc-Lys(azide)-OH were purchased from Chem-Impex; Fmoc-(PEG)2-OH was purchased from PurePEG; Thioanisole was purchased from TCl; Fmoc-protected amino acids, Oxyma pure, piperidine, ethanedithiole, anisole, acetic anhydride, DIC, TFA, TIPS, HFIP, α-chymotrypsin, fluorescamine, and doxorubicin-HCl were purchased from Sigma Aldrich. All reagents were used as received.

Peptide Synthesis and Purification

E22 Peptide System

All E22 system peptides were synthesized using an automated standard Fmoc solid-phase peptide synthesis method on a CEM Liberty Blue Automated Microwave Peptide Synthesizer. Rink amide-AM resin (100-200 mesh, 0.68 meq/g) was used as the solid support, with 1M N,N'-Diisopropylcarbodiimide as the activator, Oxyma Pure as the activator base, and 20% piperidine as the deprotectant. All amino acids were dissolved in DMF and were Fmoc protected except for Lysine where Fmoc-Lys(Boc)-OH was used. 20% acetic anhydride in DMF was used for N-terminus acetylation

Once the peptide synthesis was complete, the peptides were washed with DCM and dried. The peptides were then cleaved from the resin with a 90% TFA, 5% thioanisole, 3% ethanedithiol, and 2% anisole solution over 3 hours with agitation. The resin was filtered from the TFA solution and the peptide was precipitated with cold (-20°C) ether. Once precipitation of peptides was observed, the solution was centrifuged at 4000 RCF for 15 minutes at 4°C and the ether supernatant was discarded. The pellet was then resuspended in cold ether, probe sonicated for one minute, and centrifuged. The peptide was precipitated in ether two additional times using the same conditions. Once the ether was discarded, the peptide was placed into a desiccator to dry and subsequently purified by HPLC. The solvent was removed under reduced pressure and the peptides were lyophilized to yield a white peptide powder which was stored in a vacuum desiccator.

4F Peptide System

All 4F system peptides were synthesized using an automated standard Fmoc solid-phase peptide synthesis method on a CEM Liberty Blue Automated Microwave Peptide Synthesizer. Rink amide MBHA resin (100–200 mesh, 0.77 mmol/g) was used as the solid support.

Once peptide synthesis was complete, the peptides were cleaved from the resin with a 95% trifluoroacetic acid (TFA), 2.5% triisopropylsilane (TIPS), and 2.5% dH2O solution, followed by evaporation of the acid. The peptides were precipitated by dilution with ice-cold ether and collected via filtration. The peptides were then dissolved in acetonitrile (ACN) and precipitated with the addition of water. The peptides were precipitated in ACN and water two additional times. Purified peptides were lyophilized and stored at -80°C.

Peptide Assembly

E22 Peptide System

Purified peptides were assembled to a final concentration of 1.3 mM in acidic conditions in 40% ACN and 0.1% TFA at room temperature. The peptides were incubated for its relevant assembly times.

4F Peptide System

Purified peptides were assembled to a final concentration of 250 μM in 10% HFIP. The peptides were dissolved at 2.5 mM in hexafluoroisopropanol (HFIP) then diluted with sterile water until a 10% HFIP solution was achieved. The peptides either annealed (heated to 95°C for 30 min and cooled to 25°C at 1°C/min) or aged 2 hours at room temperature. Assemblies were then stored at 4°C.

Powder X-Ray Diffraction (XRD)

E22 Peptide System

Mature peptide nanotubes were bundled with 20 mM sulfate or magnesium at a peptide to salt ratio of 1:10. The resulting white precipitate was collected by centrifugation. The pellet was frozen and lyophilized to yield dry powder for X-ray diffraction. Powder spectra were obtained using a Bruker D8 Discover diffractometer equipped with a multi-position X, Y, Z stage, a cobalt/copper X-ray tube with Goebel mirror, and a Vantec-1 solid-state detector. The sample was placed in a zero-background holder on the stage and the spectrum obtained using Bragg-Brentano geometry. The scan step was repeated several times to maximize the diffracted intensity and minimize noise.

Nuclear Magnetic Resonance (NMR)

E22 Peptide System

Isotopically ^{13}C and ^{15}N enriched peptides were synthesized using standard Fmoc solid-phase synthesis and purified by HPLC. After assembly, sodium sulfate was added to the mature sample and pelleted at 3000 x G.[44] The pellet was frozen in liquid nitrogen and the solvent was removed by lyophilization before measurements.

All experiments were performed on a Bruker (Billerica, MA) Avance 600 spectrometer using a Bruker 4 mm HCN biosolids magic-angle spinning (MAS) probe. The MAS frequency was maintained at 10 kHz ± 2 kHz. To ensure no degradation occurred by MAS or RF heating during the experiment, cooling air was used to maintain sample temperature below -1°C. ^{13}C (150.9

MHz) CP-MAS spectra were taken before and after $^{13}C\{^{15}N\}$REDOR experiments[54,55] to ensure no change occurred in the sample. To compensate for pulse imperfections, xy8 phase cycling[56] of $^{13}C\{^{15}N\}$REDOR 4 and 8μs rotor-synchronized ^{13}C and ^{15}N π-pulses, respectively, and EXORCYCLE phase cycling[57,58] of the final ^{13}C Hahn-echo refocusing pulse is applied with 128 kHz Spinal 64 ^{1}H (600.133 MHz) decoupling.[59] $^{13}C\{^{15}N\}$REDOR data points were calculated as the sum of the center- and sideband integrated peak heights.

Transmission Electron Microscopy (TEM)

E22 Peptide System

TEM grids were prepared by pipetting 8 μL of assembled peptide solution onto the carbon side of a 200 mesh copper-carbon film grid for 1 minute. Excess peptide solution was wicked off and the grids were rinsed twice with sterile water. The grids were then stained with 8 μL of 0.75% uranyl acetate solution for 1 minute. Excess staining solution was wicked off and the grids were left to dry. Grids were imaged on either the FEI Talos 120 kV or the JOEL JEM-1400.

4F Peptide System

TEM grids were prepared by pipetting 1 μL of assembled peptide solution onto the carbon side of a 300 mesh copper-carbon film grid for 10 minutes. Excess peptide solution was wicked off and the grids were rinsed twice with sterile water. The grids were then stained twice with 2% aqueous uranyl acetate solution for 20 seconds each. Excess staining solution was wicked off and the grids were left to dry. Grids were imaged on a Tecnai T12 at 120 kV. Fiji ImageJ software (NIH)

was used for quantification and to make minor adjustments to the images for brightness and contrast.

Any experiments performed at elevated heat were left to cool to room temperature before application to the TEM grids.

Electron Diffraction (ED)

E22 Peptide System

Samples were diluted to a 0.65 mM solution of 40% ACN and 0.1% TFA. 15 µL this sample was pipetted on a 300 mesh carbon-copper grid for 1 minute and excess peptide solution was wicked off. No stain solution was applied. The grids were dried under vacuum for 5 minutes. Diffraction patterns were collected on a Talos F200X TEM at 200kV.

Circular Dichroism (CD)

E22 Peptide System

Peptide samples in their respective solvent systems were pipetted into a 0.1 mm path length quartz cuvette, and spectra were collected on a Jasco-810 Circular Dichroism Spectropolarimeter. 3 scans taken between 260 nm and 190 nm were averaged with a step size of 0.2 nm and a scanning speed of 100 nm/s.

4F Peptide System

Peptide samples in their respective solvent systems were individually diluted as needed to prevent saturation of the detector. The samples were pipetted into a 1 mm path length cuvette,

and spectra were collected on a Chirascan Plus (or Chirascan V100) Circular Dichroism spectrophotometer. For melting curves, samples were heated at 1°C/min. For nucleation rates, all peptides were assembled at 50 µM and CD at 216 nm were collected immediately after the peptide solution in HFIP was diluted into water.

Fourier Transform Infrared Spectroscopy (FT-IR)

E22 Peptide System

10 µL aliquots of assembled peptide solution were dried as thin films onto an ATR diamond crystal. Spectra was obtained at room temperature averaging 500 to 800 scans of 2 cm-1 resolution with 5 mm aperture and 4 mm/sec scanning speed, using MCT and TGS detectors. Spectra were processed with zero-filling and a cosine apodization function. IE-IR spectra were normalized to the peak height of the 12C band.

4F Peptide System

10 µL aliquots of assembled peptide solution were dried as thin films onto a horizontal attenuated total reflectance (ATR) ZnSe crystal (PerkinElmer FTIR spectrometer). Measurements were collected at room temperature in absorbance mode between 1800-1500 cm^{-1} at a resolution of 1 cm^{-1} and averaged over 32 scans.

Fluorescence Recovery After Photobleaching (FRAP)

4F Peptide System

The 4F system peptide assemblies were stained with 10% (mol) thioflavin T. Samples were diluted to a 125 µM solution of 10% HFIP and 20% glycerol was added. Videos were collected on a Zeiss 880 confocal laser-scanning microscope with an incubated enclosure, with samples equilibrating for 10 minutes at each temperature before recording.

Chymotrypsin Degradation Assays

4F Peptide System

Degradation assays: α-chymotrypsin was reconstituted at 50 µg/mL in 1 mM HCl with 2 mM CaCl2. The final reaction solution contained 50 µM pre-assembled peptide and 5 µg/mL chymotrypsin in 100 mM Tricine, 20 mM CaCl2 at pH 7.8. The solution was incubated at 30°C and measured at 1, 2, 4, 8, and 24 hour timepoints. Reactions were filtered through a 3KDa filter to remove protein before analytical HPLC (Shimadzu UFLC) and MS (Thermo Scientific LTQ-XL) were measured.

Degradation quantification: A fluorescamine assay was used to measure the concentration of free amines produced during peptide digestion. 100 µL aliquots were mixed with 33.3 µL of fluorescamine (10.8 mM in DMSO) and agitated for 5 minutes at room temperature. Dilutions of glycine under the same conditions were used to generate a calibration curve for the concentration of the free amines. Fluorescent measurements were taken on a Perkin Elmer Enspire plate reader (excitation: 387 nm, emission: 480 nm).

Doxorubicin Incorporation and Release

4F Peptide System

Loading Assays: Peptides were dissolved into a solution of DOX-HCl in HFIP and allowed to assemble on ice following the procedure detailed in the *Peptide Assembly* methods subsection. The solution was then centrifuged at 15,000 rpm for 30 min at 4°C to precipitate assembled structures. The resulting supernatant was removed and quantified from fluorescence (excitation: 488 nm, emission: 596 nm) using a Thermo Scientific Varioskan LUX plate reader.

Release Assays: Peptides were dissolved in a 500 µM solution of DOX-HCl in HFIP and allowed to assemble on ice following the procedure detailed in the *Peptide Assembly* methods subsection. Aliquots of DOX-loaded peptides were heated to 37°C for 1 hour. The solution was then centrifuged at 15,000 rpm for 30 min at 4°C to precipitate assembled structures. The resulting supernatant containing released DOX was removed. The pelleted assemblies were resuspended in 10% HFIP supplemented with 20% glycerol for CLSM imaging on a Zeiss LSM 710 using a 488 nm excitation laser. Images were collected as 15 µm z-stacks with 0.2 µm intervals. ImageJ was used for all CLSM quantification. A max intensity z-projection was performed on all images followed by an auto-threshold to select only areas with material present. The mean gray value of the selected area was then used as a relative measurement of DOX remaining in the assembly.

Cell Viability Assays: Peptides were dissolved in a 50 µM solution of DOX-HCl in HFIP and allowed to assemble on ice following the procedure detailed in the *Peptide Assembly* methods subsection. The solution was then centrifuged at 15,000 rpm for 30 min at 4°C to precipitate assembled structures. The resulting supernatant was removed and the pellets were dried under vacuum to remove any residual HFIP. The assemblies were resuspended in cell culture media before addition to the cells.

Cell Culture

4F Peptide System

Cells were plated in opaque 96-well plates with a seeding density of 3×104 cells/cm^2. Cells were plated in full cell culture media (DMEM, 10% FBS, 1% P/S) and allowed to adhere to the plate for 12 hours prior to the addition of DOX or DOX-loaded assemblies.

Doxorubicin Dose Response Curves: A 50 mM stock solution of DOX-HCl in molecular biology grade water was prepared immediately prior to the start of the assay. DOX standards were then prepared with the stock solution in full cell culture media at concentrations ranging from 3 nM to 50 µM. Following cell plating and adherence to the plate, the culture media was removed and replaced with DOX-containing media or a no-drug control. Standards were run in triplicate, and cell viability was measured at 24 and 48 hours using the CellTiter-Glo 2.0 Cell Viability Assay (Promega, G9241). Luminescence values were measured using a Biotek Synergy HTX Multi-Mode Reader in luminescence mode, with a 1mm read height and a 1 second integration time.

Following this, all data analysis was performed in GraphPad Prism 9. Raw luminescence values from DOX dose response assays were first normalized to the mean of the no-drug control wells. This value was set to 100% viability. The data was then fit using the built-in Prism non-linear fit "[Inhibitor] vs Normalized Response – Variable Slope" using a standard Least-Squares regression. All replicates were used for the fitting and data points came from 3 independent experiments. Equations from the curve fits were used to calculate effective doses from cell viability results with peptides. The percent release was calculated by comparing the effective dose to the total incorporated DOX.

Killing Assays: DOX-loaded structures were prepared following the procedure detailed in the *Doxorubicin Incorporation and Release* methods subsection. Immediately prior to the start of the assay, dried structures were resuspended in the cell culture media to a final peptide concentration of 250 μM. Following cell plating and adherence to the plate, the culture media was removed and replaced with solutions of DOX-loaded assemblies. Peptide assemblies were run in triplicate, and cell viability was measured at 24 and 48 hours using the CellTiter-Glo 2.0 Cell Viability Assay.

Live/Dead Assays: Cells were incubated with DOX-loaded structures for 1 and 48 hours. The cell culture media was then removed and replaced with PBS buffer containing 2 μM Calcein AM and 3 μM Propidium iodide (Invitrogen). Cells were labeled for 30 minutes at room temperature followed by imaging using a GE INCell Analyzer 2200 high-content microscope at 10x using FITC and Texas Red filter sets.

Following this, assay images were processed using Fiji/ImageJ, v1.53s (NIH). Low magnification tiled fluorescent images were loaded into Fiji and first stitched into one final image for each well using the “Grid/Collection” stitching plug-in.

References

[1] E. Pieters, B. J. G.; Eldijk, M. B. van; M. Nolte, R. J.; Mecinović, J. Natural Supramolecular Protein Assemblies. *Chemical Society Reviews* **2016**, *45* (1), 24–39. https://doi.org/10.1039/C5CS00157A.

[2] Chiesa, G.; Kiriakov, S.; Khalil, A. S. Protein Assembly Systems in Natural and Synthetic Biology. *BMC Biology* **2020**, *18* (1). https://doi.org/10.1186/s12915-020-0751-4.

[3] Qiu, T.; Liu, Q.; Chen, Y.-X.; Zhao, Y.-F.; Li, Y.-M. Aβ42 and Aβ40: Similarities and Differences. *Journal of Peptide Science* **2015**, *21* (7), 522–529. https://doi.org/10.1002/psc.2789.

[4] Sabate, R. When Amyloids Become Prions. *Prion* **2014**, *8* (3), 233–239. https://doi.org/10.4161/19336896.2014.968464.

[5] Chiti, F.; Webster, P.; Taddei, N.; Clark, A.; Stefani, M.; Ramponi, G.; Dobson, C. M. Designing Conditions for in Vitro Formation of Amyloid Protofilaments and Fibrils. *Proceedings of the National Academy of Sciences* **1999**, *96* (7), 3590–3594. https://doi.org/10.1073/pnas.96.7.3590.

[6] Ji, G.; Sunde, M.; Jones, J. A.; Campbell Id; Dobson, C. Amyloid Fibril Formation by an SH3 Domain. *Proceedings of the National Academy of Sciences of the United States of America* **1998**, *95* (8), 4224–4228. https://doi.org/10.1073/pnas.95.8.4224.

[7] Dobson, C. M. Protein Misfolding, Evolution and Disease. *Trends in Biochemical Sciences* **1999**, *24* (9), 329–332. https://doi.org/10.1016/s0968-0004(99)01445-0.

[8] Hsieh, M.-C.; Lynn, D. G.; Grover, M. A. Kinetic Model for Two-Step Nucleation of Peptide Assembly. *The Journal of Physical Chemistry B* **2017**, *121* (31), 7401–7411. https://doi.org/10.1021/acs.jpcb.7b03085.

[9] Hughes, S. A.; Wang, F.; Wang, S.; Kreutzberger, M. A. B.; Osinski, T.; Orlova, A.; Wall, J. S.; Zuo, X.; Egelman, E. H.; Conticello, V. P. Ambidextrous Helical Nanotubes from Self-Assembly of Designed Helical Hairpin Motifs. *Proceedings of the National Academy of Sciences* **2019**, *116* (29), 14456–14464. https://doi.org/10.1073/pnas.1903910116.

[10] Tycko, R.; Sciarretta, K. L.; Orgel, J.; Meredith, S. C. Evidence for Novel β-Sheet Structures in Iowa Mutant β-Amyloid Fibrils. *Biochemistry* **2009**, *48* (26), 6072–6084. https://doi.org/10.1021/bi9002666.

[11] Wang, Q.; Yau, W.; Tycko, R. Structural Evolution of Iowa Mutant β-Amyloid Fibrils from Polymorphic to Homogeneous States under Repeated Seeded Growth. *Journal of the American Chemical Society* **2011**, *133* (11), 4018–4029. https://doi.org/10.1021/ja109679q.

[12] Qiang, W.; Yau, W.-M.; Luo, Y.; Mattson, M. P.; Tycko, R. Antiparallel β-Sheet Architecture in Iowa-Mutant β-Amyloid Fibrils. *Proceedings of the National Academy of Sciences* **2012**, *109* (12), 4443–4448. https://doi.org/10.1073/pnas.1111305109.

[13] Chen, B.; Newnam, G. P.; Chernoff, Y. O. Prion Species Barrier between the Closely Related Yeast Proteins Is Detected despite Coaggregation. *Proceedings of the National Academy of Sciences* **2007**, *104* (8), 2791–2796. https://doi.org/10.1073/pnas.0611158104.

[14] Chen, B.; Bruce, K. L.; Newnam, G. P.; Gyoneva, S.; Romanyuk, A. V.; Chernoff, Y. O. Genetic and Epigenetic Control of the Efficiency and Fidelity of Cross-Species Prion Transmission.

Molecular Microbiology **2010**, *76* (6), 1483–1499. https://doi.org/10.1111/j.1365-2958.2010.07177.x.

[15] Grizel, A. V.; Rubel, A. A.; Chernoff, Y. O. Strain Conformation Controls the Specificity of Cross-Species Prion Transmission in the Yeast Model. *Prion* **2016**, *10* (4), 269–282. https://doi.org/10.1080/19336896.2016.1204060.

[16] Inge-Vechtomov, S.; Zhouravleva, G.; Chernoff, Y. O. Biological Roles of Prion Domains. *Prion* **2007**, *1* (4), 228–235. https://doi.org/10.4161/pri.1.4.5059.

[17] Tessier, P. M.; Lindquist, S. Unraveling Infectious Structures, Strain Variants and Species Barriers for the Yeast Prion [PSI+]. *Nature Structural & Molecular Biology* **2009**, *16* (6), 598–605. https://doi.org/10.1038/nsmb.1617.

[18] Wickner, R. B. Prions: Proteins as Genes and Infectious Entities. *Genes & Development* **2004**, *18* (5), 470–485. https://doi.org/10.1101/gad.1177104.

[19] Tuite, M. F.; Cox, B. S. Propagation of Yeast Prions. *Nature Reviews Molecular Cell Biology* **2003**, *4* (11), 878–890. https://doi.org/10.1038/nrm1247.

[20] Houston, F.; Andréoletti, O. Animal Prion Diseases: The Risks to Human Health. *Brain Pathology* **2019**, *29* (2), 248–262. https://doi.org/10.1111/bpa.12696.

[21] Kupfer, L.; Hinrichs, W.; Groschup, M. Prion Protein Misfolding. *Current Molecular Medicine* **2009**, *9* (7), 826–835. https://doi.org/10.2174/156652409789105543.

[22] Mankar, S.; Anoop, A.; Sen, S.; Maji, S. K. Nanomaterials: Amyloids Reflect Their Brighter Side. *Nano Reviews* **2011**, *2* (1), 6032. https://doi.org/10.3402/nano.v2i0.6032.

[23] Kollmer, M.; Close, W.; Funk, L.; Rasmussen, J.; Bsoul, A.; Schierhorn, A.; Schmidt, M.; Sigurdson, C. J.; Jucker, M.; Fändrich, M. Cryo-EM Structure and Polymorphism of Aβ Amyloid Fibrils Purified from Alzheimer's Brain Tissue. *Nature Communications* **2019**, *10* (1). https://doi.org/10.1038/s41467-019-12683-8.

[24] *Prion diseases*. www.niaid.nih.gov. https://www.niaid.nih.gov/diseases-conditions/prion-diseases.

[25] Jucker, M.; Walker, L. C. Self-Propagation of Pathogenic Protein Aggregates in Neurodegenerative Diseases. *Nature* **2013**, *501* (7465), 45–51. https://doi.org/10.1038/nature12481.

[26] Walker, L. C.; LeVine, H.; Mattson, M. P.; Jucker, M. Inducible Proteopathies. *Trends in Neurosciences* **2006**, *29* (8), 438–443. https://doi.org/10.1016/j.tins.2006.06.010.

[27] Collinge, J.; Whitfield, J.; McKintosh, E.; Beck, J.; Mead, S.; Thomas, D. J.; Alpers, M. P. Kuru in the 21st Century--an Acquired Human Prion Disease with Very Long Incubation Periods. *Lancet (London, England)* **2006**, *367* (9528), 2068–2074. https://doi.org/10.1016/S0140-6736(06)68930-7.

[28] Cortelli, P.; Gambetti, P.; Montagna, P.; Lugaresi, E. Fatal Familial Insomnia: Clinical Features and Molecular Genetics. *Journal of Sleep Research* **1999**, *8* (S1), 23–29. https://doi.org/10.1046/j.1365-2869.1999.00005.x.

[29] Caimi, F.; Giuliano Zanchetta. Twisted Structures in Natural and Bioinspired Molecules: Self-Assembly and Propagation of Chirality across Multiple Length Scales. *ACS Omega* **2023**, *8* (20), 17350–17361. https://doi.org/10.1021/acsomega.3c01822.

[30] Rich, A.; Zhang, S. Z-DNA: The Long Road to Biological Function. *Nature Reviews Genetics* **2003**, *4* (7), 566–572. https://doi.org/10.1038/nrg1115.

[31] Macnab, R. M.; Ornston, M. K. Normal-To-Curly Flagellar Transitions and Their Role in Bacterial Tumbling. Stabilization of an Alternative Quaternary Structure by Mechanical Force. *Journal of Molecular Biology* **1977**, *112* (1), 1–30. https://doi.org/10.1016/s0022-2836(77)80153-8.

[32] Xing, Q.; Zhang, J.; Xie, Y.; Wang, Y.; Qi, W.; Rao, H.; Su, R.; He, Z. Aromatic Motifs Dictate Nanohelix Handedness of Tripeptides. *ACS Nano* **2018**, *12* (12), 12305–12314. https://doi.org/10.1021/acsnano.8b06173.

[33] Martial, B.; Lefèvre, T.; Buffeteau, T.; Auger, M. Vibrational Circular Dichroism Reveals Supramolecular Chirality Inversion of α-Synuclein Peptide Assemblies upon Interactions with Anionic Membranes. *ACS Nano* **2019**, *13* (3), 3232–3242. https://doi.org/10.1021/acsnano.8b08932.

[34] Xue, S.; Xing, P.; Zhang, J.; Zeng, Y.-F.; Zhao, Y. Diverse Role of Solvents in Controlling Supramolecular Chirality. *Chemistry Europe* **2019**, *25* (31), 7426–7437. https://doi.org/10.1002/chem.201900714.

[35] Wang, L.; Dong, H.; Li, Y.; Liu, R.; Wang, Y.; Bisoyi, H. K.; Sun, L.-D.; Yan, C.-H.; Li, Q. Luminescence-Driven Reversible Handedness Inversion of Self-Organized Helical Superstructures Enabled by a Novel Near-Infrared Light Nanotransducer. *Advanced Materials* **2015**, *27* (12), 2065–2069. https://doi.org/10.1002/adma.201405690.

[36] Chou, K.-C.; Pottle, M. S.; Némethy, G.; Ueda, Yuzo; Scheraga, H. A. Structure of β-Sheets. *Journal of Molecular Biology* **1982**, *162* (1), 89–112. https://doi.org/10.1016/0022-2836(82)90163-2.

[37] Wang, L.; O'Connell, T.; Tropsha, A.; Hermans, J. Molecular Simulations of β-Sheet Twisting. *Journal of Molecular Biology* **1996**, *262* (2), 283–293. https://doi.org/10.1006/jmbi.1996.0513.

[38] Chou, K.; Scheraga, H. A. Origin of the Right-Handed Twist of Beta-Sheets of Poly(LVal) Chains. *Proceedings of the National Academy of Sciences of the United States of America* **1982**, *79* (22), 7047–7051. https://doi.org/10.1073/pnas.79.22.7047.

[39] Jain, A.; Kassem, S.; Fisher, R. S.; Wang, B.; Li, T.-D.; Wang, T.; He, Y.; Elbaum-Garfinkle, S.; Ulijn, R. V. Connected Peptide Modules Enable Controlled Co-Existence of Self-Assembled Fibers inside Liquid Condensates. *Journal of the American Chemical Society* **2022**, *144* (33), 15002–15007. https://doi.org/10.1021/jacs.2c05897.

[40] Jasco. *Circular Dichroism Spectroscopy - JASCO*. JASCO Inc. https://jascoinc.com/learning-center/theory/spectroscopy/circular-dichroism-spectroscopy/.

[41] Micsonai, A.; Wien, F.; Kernya, L.; Lee, Y.-H.; Goto, Y.; Réfrégiers, M.; Kardos, J. Accurate Secondary Structure Prediction and Fold Recognition for Circular Dichroism Spectroscopy. *Proceedings of the National Academy of Sciences* **2015**, *112* (24), E3095–E3103. https://doi.org/10.1073/pnas.1500851112.

[42] Yan, X.; Zhu, P.; Li, J. Self-Assembly and Application of Diphenylalanine-Based Nanostructures. *Chemical Society Reviews* **2010**, *39* (6), 1877. https://doi.org/10.1039/b915765b.

[43] Mehta, A.; Kun Ping Lu; W. Seth Childers; Liang, Y.; Dublin, S. N.; Dong, J.; Snyder, J. P.; Sai Venkatesh Pingali; Pappannan Thiyagarajan; Lynn, D. G. Facial Symmetry in Protein Self-Assembly. *Journal of the American Chemical Society* **2008**, *130* (30), 9829–9835. https://doi.org/10.1021/ja801511n.

[44] Lu, K. P.; Guo, L.; Mehta, A. K.; Childers, W. S.; Dublin, S. N.; Skanthakumar, S.; Conticello, V. P.; Thiyagarajan, P.; Apkarian, R. P.; Lynn, D. G. Macroscale Assembly of Peptide Nanotubes. *Chemical Communications* **2007**, No. 26, 2729–2729. https://doi.org/10.1039/b701029j.

[45] Ling, Y.; Pingali, S. V.; Jogalekar, A. S.; Snyder, J. P.; Thiyagarajan, P.; Lynn, D. G. Cross-Strand Pairing and Amyloid Assembly. *Biochemistry* **2008**, *47* (38), 10018–10026. https://doi.org/10.1021/bi801081c.

[46] Liang, Y.; Lynn, D. G.; Berland, K. M. Direct Observation of Nucleation and Growth in Amyloid Self-Assembly. *Journal of the American Chemical Society* **2010**, *132* (18), 6306–6308. https://doi.org/10.1021/ja910964c.

[47] Anthony, N. R.; Mehta, A. K.; Lynn, D. G.; Berland, K. M. Mapping Amyloid-β(16-22) Nucleation Pathways Using Fluorescence Lifetime Imaging Microscopy. *Soft Matter* **2014**, *10* (23), 4162–4172. https://doi.org/10.1039/c4sm00361f.

[48] Balbach, J. J.; Ishii, Y.; Antzutkin, O. N.; Leapman, R. D.; Rizzo, N. W.; Dyda, F.; Reed, J.; Tycko, R. Amyloid Fibril Formation by Aβ16-22, a Seven-Residue Fragment of the Alzheimer's β-Amyloid Peptide, and Structural Characterization by Solid State NMR†. *Biochemistry* **2000**, *39* (45), 13748–13759. https://doi.org/10.1021/bi0011330.

[49] Lee, D.; Redfern, O.; Orengo, C. Predicting Protein Function from Sequence and Structure. *Nature Reviews Molecular Cell Biology* **2007**, *8* (12), 995–1005. https://doi.org/10.1038/nrm2281.

[50] Cheng, Y.; Koh, L.-D.; Li, D.; Ji, B.; Han, M.-Y.; Zhang, Y.-W. On the Strength of β-Sheet Crystallites of Bombyx Mori Silk Fibroin. *Journal of the Royal Society Interface* **2014**, *11* (96), 20140305. https://doi.org/10.1098/rsif.2014.0305.

[51] Wang, F.-B.; Gnewou, O. M.; Wang, S.-Y.; Osinski, T.; Zuo, X.; Egelman, E. H.; Conticello, V. P. Deterministic Chaos in the Self-Assembly of β Sheet Nanotubes from an Amphipathic Oligopeptide. *Matter* **2021**, *4* (10), 3217–3231. https://doi.org/10.1016/j.matt.2021.06.037.

[52] Ulijn, R. V.; Lampel, A. Order/Disorder in Protein and Peptide-Based Biomaterials. *Israel Journal of Chemistry* **2019**, *60* (12), 1129–1140. https://doi.org/10.1002/ijch.201900051.

[53] Shen, Y.; Wang, Y.; Hamley, I. W.; Qi, W.; Su, R.; He, Z. Chiral Self-Assembly of Peptides: Toward the Design of Supramolecular Polymers with Enhanced Chemical and Biological Functions. *Progress in Polymer Science* **2021**, *123*, 101469. https://doi.org/10.1016/j.progpolymsci.2021.101469.

[54] Gullion, T.; Schaefer, J. Rotational-Echo Double-Resonance NMR. *Journal of Magnetic Resonance (1969)* **1989**, *81* (1), 196–200. https://doi.org/10.1016/0022-2364(89)90280-1.

[55] Gullion, T.; Schaefer, J. Detection of Weak Heteronuclear Dipolar Coupling by Rotational-Echo Double-Resonance Nuclear Magnetic Resonance. *Advances in magnetic and optical resonance* **1989**, 57–83. https://doi.org/10.1016/b978-0-12-025513-9.50009-4.

[56] Gullion, T.; Baker, D. B.; Conradi, M. S. New, Compensated Carr-Purcell Sequences. *Journal of Magnetic Resonance (1969)* **1990**, *89* (3), 479–484. https://doi.org/10.1016/0022-2364(90)90331-3.

[57] Rance, M.; R. Andrew Byrd. Obtaining High-Fidelity Powder Spectra in Anisotropic Media: Phase-Cycled Hahn Echo Spectroscopy. *Journal of magnetic resonance* **1983**, *52* (2), 221–240. https://doi.org/10.1016/0022-2364(83)90190-7.

[58] Sinha, N.; Schmidt-Rohr, K.; Hong, M. Compensation for Pulse Imperfections in Rotational-Echo Double-Resonance NMR by Composite Pulses and EXORCYCLE. *Journal of Magnetic Resonance* **2004**, *168* (2), 358–365. https://doi.org/10.1016/j.jmr.2004.03.025.

[59] Fung, B. M.; Khitrin, A. K.; Ermolaev, K. An Improved Broadband Decoupling Sequence for Liquid Crystals and Solids. *Journal of Magnetic Resonance* **2000**, *142* (1), 97–101. https://doi.org/10.1006/jmre.1999.1896.

Additional References:

[W] Klawa, S. J.; **Lee, Michelle**.; Riker, K. D.; Jian, T.; Wang, Q.; Bhonge, S.; Gao, Y.; Childers, W. S.; Omosun, T. O.; Mehta, A. K.; Lynn, D. G.; Freeman, R. Uncovering Supramolecular Chirality Codes for the Design of Tunable Biomaterials. *Nature Communications*. Submitted.

[X] Data collection and image credits to John Bacsa from the X-Ray Crystallography Lab at Emory University, Department of Chemistry